



Preparation of eco-friendly graphene oxide from agricultural wastes for water treatment

Hebat-Allah S. Tohamy^a, Badawi Anis^b, Mohamed A. Youssef^c, Amira E.M. Abdallah^c, Mohamed El-Sakhawy^a, Samir Kamel^{a,*}

^aCellulose and Paper Department, National Research Centre, 33 El-Bohouth Str., P.O. 12622, Dokki Giza, Egypt, Tel. +20 1098659262; emails: samirki@yahoo.com (S. Kamel), hebasarhan89@yahoo.com (H.-A.S. Tohamy), elsakhawym@gmail.com (M. El-Sakhawy)

^bSpectroscopy Department, Physics Division, National Research Centre, 33 El Bohouth Str., P.O. 12622, Dokki Giza, Egypt, email: badawi.ali@gmail.com (B. Anis)

^cDepartment of Chemistry, Faculty of Science, Helwan University, Egypt, emails: moramoon1711@gmail.com (M.A. Youssef), miroemao@yahoo.com (A.E.M. Abdallah)

Received 18 July 2019; Accepted 3 February 2020

ABSTRACT

In the present study, an eco-friendly graphene oxide (GO) were successfully synthesized via single-step from different agricultural wastes by oxidation under muffled atmosphere condition. The synthesized adsorbents were characterized by Fourier transform infrared spectroscopy, scanning electron microscopy, energy-dispersive X-ray spectroscopy, transmission electron microscope, and Raman spectroscopy. A simple adsorption method was designed for the removal of Ni(II) by the utilization of GO. The different parameters were optimized such as temperature, concentrations, and time. Among the investigated agricultural wastes, the highest removal of Ni(II) (up to 85.06%) was established for GO obtained from sugarcane bagasse. All the prepared samples from different agricultural wastes showed a good agreement with the Langmuir isotherm model as the obtained regression constant value (R^2) is found to be 0.9. Kinetic studies revealed that the prepared samples are well fitted with the pseudo-second-order due to the surface processes involving chemisorption adsorption of Ni(II). The results showed the applicability of GO obtained from agricultural wastes as a low-cost adsorbent for Ni(II) from aqueous solution.

Keywords: Agricultural wastes; Graphene oxide; Ni(II) Adsorption; Thermodynamic analysis

1. Introduction

Contamination of water is a worldwide problem for the environment and human health [1]. During the last decades, contamination of drinking water has emerged as a serious problem. Drinking water can be contaminated through the release of natural organic matters and leakage of heavy metals ions as well. In general, consumption of contaminated water considered as one of the major causes of the 2.2 million diarrhea disease death occurring annually, mostly in

children. Also; contaminated water causes cancer, dermatitis, liver sicknesses, and nasal ulceration [2].

Therefore, several methods have been employed for water purification including precipitation, electro-winning, electro-coagulation, cementation, ion exchange, reverse osmosis, distillation, and adsorption [3]. Among them, adsorption method received considerable interest because of its high adsorption capacity for metal ions and it is cost effective [3]. A large number of adsorbents namely, diatomite, zeolites, granulated ferric hydroxide, and ceramics have been used [4]. The deployed utilization of these methods and

* Corresponding author.

adsorbents is limited due to self-contamination, huge power necessities, and utilization of intense resources, low volume concentration removal of metal ions and not being economically applicable [5,6]. Nanotechnology has opened an opportunity for researching water purification by a new economically viable material [1,6]. Carbon-based nanosorbents such as graphene (G), graphene oxide (GO), and carbon nanotubes (CNTs) have been widely used for wastewater purification [7]. Carbon allotropes namely, G, GO, and CNTs in nano size have been used for adsorption experiments to separate organic pollutants and metals due to their inherent large surface area [8].

GO is the oxidized form of G decorated with reactive oxygen functional groups, which make it the right choice for use in many applications [8]. Oxygen-containing functional groups in GO such as carboxyl ($-\text{COOH}$), carbonyl ($-\text{C}=\text{O}$), and phenol groups at the sheet edges, and epoxy ($\text{C}-\text{O}-\text{C}$), and hydroxyl ($-\text{OH}$) groups on the basal plane give the hydrophilic properties to GO [9].

Accordingly, GO has good water-dispersibility and versatile surface modification [8]. The GO surface is highly heterogeneous with both hydrophobic pristine graphene regions and hydrophilic oxidized areas [8]. Recently, GO has emerged as a strong powerful sorbent candidate with effective antibacterial activity [10].

Chemically modified GO, namely (ethylenediamine-tetraacetic acid) EDTA-GO showed high adsorption capacity of 479 mg/g for Pb(II). While GO modified with ferrite magnetic nanoparticles showed adsorption capacity of 488 mg/g for Pb(II) [11]. Modified reduced graphene oxide (rGO) by microbe and titanium dioxide have been used for Pb(II) and Cu(II) removal [12]. In addition, GO has been used as high-performance phosphate removal [13], organic surfactant removal [14], dyes removal, and for recovery of noble metals [15]. Sponge-like polysiloxane-graphene oxide (PS-GO) gel has shown an adsorption capacity of 256 mg/g for Pb(II) [16].

Hummers' method is the original method to synthesize GO. In this method, potassium chlorate was added to the slurry of graphite in fuming nitric acid. This procedure involves the generation of toxic gases such as NO_2 , N_2O_4 , and ClO_2 which are explosive [17]. Agricultural wastes are the residues from the first processing of raw agricultural products such as fruits, vegetables, and crops. These wastes can be recycled into useful products for controlling environment pollution [18].

The development of new carbon allotropes derived from agricultural wastes is of significant interest [6]. Where the agricultural wastes can be easily recycled into valuable products, requires lesser chemical reagents and are eco-friendly for removing toxic metal ions from wastewater [5]. Due to their low cost and eco-friendly properties, after these natural sorbents have been exhausted, they can be thrown down safely [6].

Sugar cane bagasse and corn residues are pyrolyzed to synthesis carbon nanomaterials (CNMs) including CNTs [19]. Graphene, carbon nanotube and their composites were fabricated from rice husk by one-step microwave plasma irradiation [20]. Simultaneous activation-graphitization is a cost-effective and easy route to synthesis a large surface area porous graphene from coconut shell using (FeCl_3) and

(ZnCl_2) as activating agent [21]. Novel pyrolysis system was applied to prepare CNTs from hydro chars of rice straw and rice straw pulp. It was found that the type of rice straw precursor plays a significant effect on the shape and size of producing CNTs [22].

Liquid-phase exfoliation (ultra-sonication) of the pyrolyzed residue in the furnace at 400°C – $1,200^\circ\text{C}$ produced graphene without need for pretreatment with Fe or previous oxidation stages. Graphene is separated from the liquid phase with a degree of carbon purity greater than 95% without expensive purification processes [23]. When starting polymers were heated either continuously in air or in a cyclic manner with small amount of air at about 240°C , CNTs were formed only in unmodified plant cell wall agro wastes (not by using purified lignin and cellulose), because the nanometer-scale arrangement of the chemical components in plant cell walls may play a critical role [24].

In this study, the syntheses of eco-friendly and low cost GO by direct oxidation of agricultural wastes under muffled atmosphere was reported. Agricultural wastes as bagasse, rice straw, sawdust and black liquor, which usually burned or dumped off on landfill causing environmental problems, were utilized to prepare a value added product (GO) by a simple method. Furthermore, the obtained GO has been used in the removal of Ni(II) from water. The structural characteristics of the obtained product are confirmed by Fourier transform infrared spectroscopy (FT-IR), scanning electron microscopy (SEM), transmission electron microscopy (TEM), and Raman spectroscopy. In addition, the parameters affecting the removal efficiency towards Ni(II) have been investigated in detail.

2. Materials and methods

2.1. Materials

Sugarcane bagasse (SCB) and black liquor (BL) were kindly provided from Quena Company for Paper Industry, Egypt. Rice straw (RS) from the Nile valley was used for this study. The straw (leaves and stems) were collected and the seeds were separated. Mature beech pinewood sawdust (MW) was obtained from a local wood processing factory. The lignocellulosic materials (SCB, RS, MW, and lignin) were air-dried, homogenized to avoid compositional differences between batches. SCB, RS, and MW were grinding to mesh size 450 micron. Ferrocene (F) was purchased from Sisco research laboratories Pvt. Ltd., (India). Other chemicals used were of analytical grades and used without further purification.

2.2. Synthesis of GO from different agricultural wastes

GO was firstly prepared by oxidation of SCB with ferrocene at 300°C in muffled conditions [17]. A mixture of 0.5 g (SCB, RS, MW, or L) with 0.1 g ferrocene was charged into a muffle furnace at 300°C for 10 min under atmospheric conditions. In another trial, GO was prepared without ferrocene. The prepared GO samples were denoted by SCB/F, RS/F, MW/F, and L/F for the samples SCB, RS, MW, and L, respectively. The as-produced black solid was collected at room temperature and subjected to further analysis. Fig. 1 shows the aqueous dispersion of GO obtained from SCB/F.

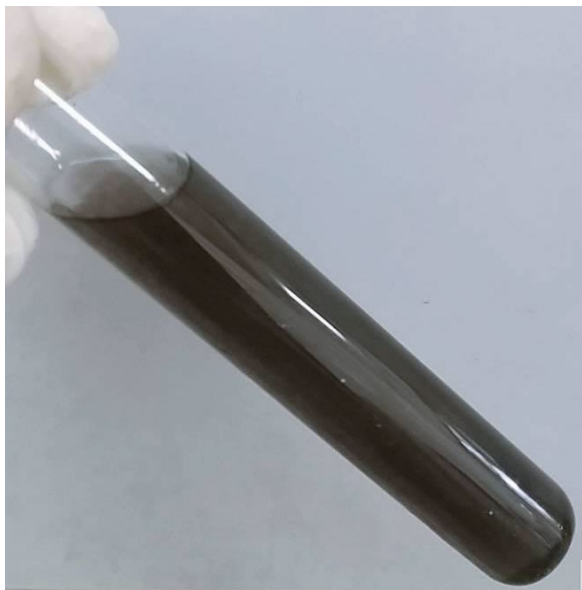


Fig. 1. Dark brown dispersion of GO from SCB/F.

2.3. Ni(II) adsorption study

Samples of Ni(II) solutions were prepared by adding 20 mg of GOs in 20 mL of Ni(II) solution with known initial concentration (15 mg/L) and stirred at different time intervals to study the effect of contact time. The effect of temperature on adsorption capacity of Ni(II) on GO surface was elucidated from 298 to 328 K. All adsorption experiments were performed at fixed contact time, that is, 30 min. The removal experiments were performed using various initial concentrations from 15, 20, 25, and 30 mg/L at fixed contact time, that is, 30 min and 298 K to study the effect of the initial concentration of Ni(II). The final metal ions concentrations were measured using an atomic absorption spectrophotometer. The removal efficiency percent ($R\%$) for sorbents toward metals ions were calculated by the following equation [25]:

$$R\% = \frac{C_0 - C_t}{C_0} \times 100 \quad (1)$$

where C_0 is the initial concentration of Ni(II) impurity in water and C_t is the final concentration of Ni(II) impurity in water after treatment.

2.4. Characterization

FT-IR spectroscopy was carried out using a Mattson 5000 spectrometer (Unicam, UK) by KBr technique. In addition, the samples were investigated using scanning electron microscopy (SEM), Quanta 250 FEG. Energy dispersive X-ray (EDX) was conducted using the EDX unit attached to the SEM. Furthermore, transmission electron microscope (TEM) images were taken with a JEOL JEM-2100 electron microscope at an acceleration voltage of 120 kV. Moreover, Raman Spectroscopy was performed using a WITTEC Alpha-300 Raman confocal microscope, (Germany). The spectra

were recorded with a 532 nm excitation wavelength. Atomic absorption PerkinElmer 3110, USA was used to quantify the amount of metal ions.

3. Results and discussion

3.1. Raman spectroscopy

Fig. 2 shows the Raman spectra of GO synthesized from different agricultural wastes. From the figure, it can see clearly the presence of the G-bands which arising from the stretching of sp^2 carbon, graphitic hexagon-pinch mode. The G-band is located at 1,582; 1,582; 1,583; 1,571; 1,584; 1,582; 1,572; and 1,571 cm^{-1} for SCB/F, SCB, RS/F, RS, MW/F, MW, L/F, and L, respectively [25,26]. The D-band appears due to the presence of disorder in atomic arrangement, that is, impurities and edges [25]. The characteristic D-bands (arising from the stretching of sp^3 carbons of graphene sheets) located at 1,378; 1,363; 1,324; 1,357; 1,369; 1,359; 1,356; and 1,359 cm^{-1} for SCB/F, SCB, RS/F, RS, MW/F, MW, L/F, and L, respectively [25,26]. Thus, smaller I_D/I_G peak intensity ratios are assigned to lower defects/disorders [26]. The calculated I_D/I_G value is less than 2 indicating the nanocrystalline graphitic nature of the material and is consistent with many reported values. The slight increase in I_D/I_G value suggests the formation of a high level of disordered structure [27]. The calculated I_D/I_G ratios for the samples are listed in Table 1. From Table 1, it is clear that the I_D/I_G ratio in the case of SCB/F is the lowest ratio among other samples. In general, the increase of I_D/I_G ratio is attributed to the decrease in average size of the sp^2 domains upon variation of agro-waste used and due to the increase of the defects density, clearly indicating that during the oxidation process the formation of vacancies and defects in the carbon lattice, such as five and seven-member carbon rings, took place [28]. Raman spectra show an intensity ratio of I_D/I_G centered between 0.598 and 0.805 for the prepared samples which is in line with previous investigations (~ 0.76) [17].

On the other hand, the G-band was much wider in the case of the SCB/F spectrum compared with other samples. This can be attributed to the structural imperfections induced by the attachment of higher amount of hydroxyl and/or epoxy groups on the surface of the SCB/F [28]. This result has been confirmed by measuring the relative absorbance (RA) of the OH, C=O, C–OH, and C–O–C absorption bands by FT-IR data (FT-IR section).

The number of layers of the resulting GOs can be identified from the position and the width of the 2D Raman active mode [28]. The position of the 2D-band is located at about 2,679 cm^{-1} in the case of single layer graphene. For the multilayer graphene (2–4 layers), the position shifts to higher wave number by ≈ 19 cm^{-1} along with peak broadening [29]. Furthermore, the I_{2D}/I_G intensity ratios for single-, double-, triple-, and multi- (>4) layer G are typically >1.6, 0.8, 0.30, and 0.07, respectively [30]. Here, all the GO samples synthesized from the various starting materials showed a 2D band located at 2,830–2,920 cm^{-1} , indicating the presence of multi-layer GO sheets in the samples. Moreover, none of the samples showed $I_{2D}/I_G > 0.5$; this ratio was found to be <0.3 for all samples. Therefore, all the GO sheets synthesized by this proposed method showed multilayer

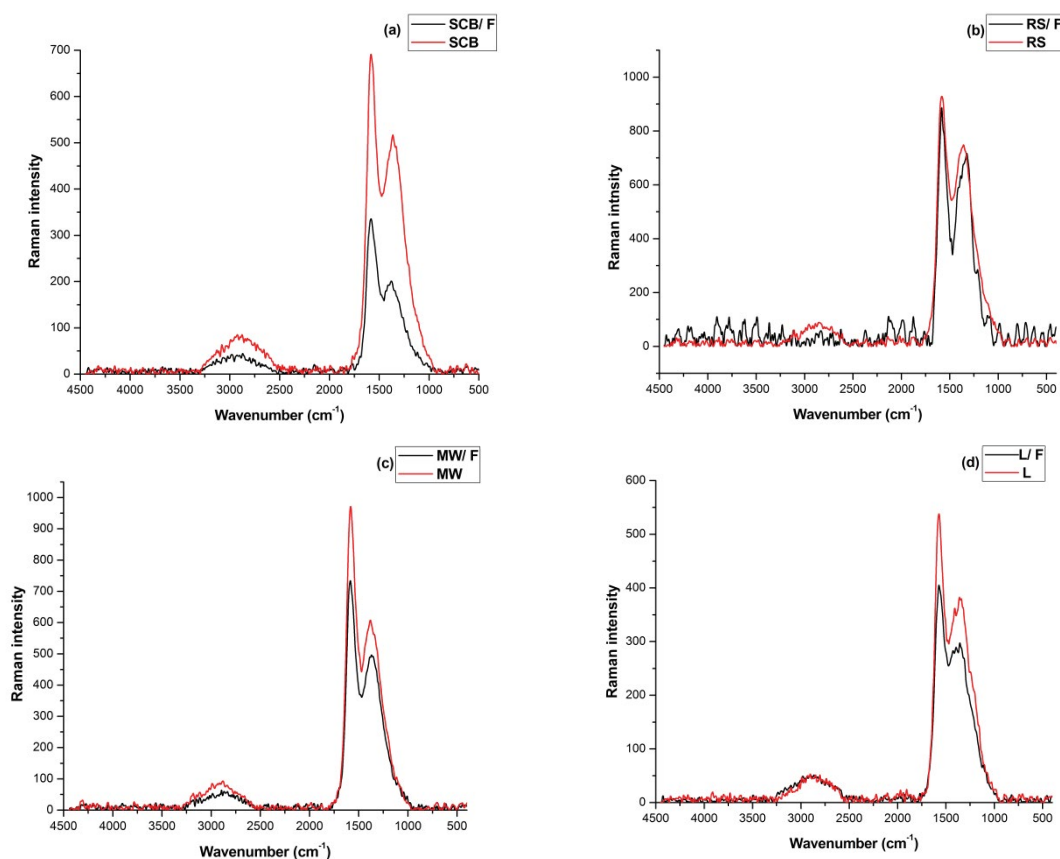


Fig. 2. Raman spectra of (a) SCB/F and SCB, (b) RS/F and RS, (c) MW/F and MW, and (d) L/F and L.

Table 1
Raman spectra peak positions, I_D/I_G and I_{2D}/I_G values of GO prepared from different agro wastes

Sample	D band (cm^{-1})	G band (cm^{-1})	FWHM G band (cm^{-1})	2D band (cm^{-1})	FWHM 2D band (cm^{-1})	I_D/I_G	I_{2D}/I_G
SCB/F	1,378	1,582	92	2,926	417	0.598	0.10
SCB	1,363	1,582	78	2,877	475	0.747	0.25
L/F	1,356	1,572	75	2,855	376	0.734	0.12
L	1,359	1,571	87	2,902	376	0.7106	0.09
RS/F	1,324	1,583	84	2,830	83	0.808	–
RS	1,357	1,582	77	2,852	263	0.805	0.081
MW/F	1,369	1,584	72	2,894	306	0.6756	0.066
MW	1,359	1,571	74	2,880	315	0.6138	0.091

structures [29]. The variation between the prepared samples types in Raman results due to the nanometer-scale arrangement of the chemical components in plant cell walls may play a critical role [24]. Our Raman results match state of Somanathan et al. [17] method in which the spectrum of their GO displays the two D and G bands at 1,358 and 1,585 cm^{-1} . Indicate the clear sp^2 -hybridized carbon in the observed GO.

3.2. FT-IR analysis

Fig. 3 shows the FT-IR spectra of GO synthesized from different agricultural wastes. The FT-IR spectrum of GO

confirms the introduction of oxygen-containing groups such as functional hydroxyl, epoxy, and carboxylic groups upon oxidation of agricultural wastes. For investigated samples, the peak centered at 1,710–1,735 cm^{-1} is attributed to stretching vibration modes of C=O which is either located in carboxyl and carbonyl groups or on the edge of GO [17,30]. While the peak centered at 1,594–1,613 cm^{-1} are assigned the C=C bonds [30,31].

In addition, the bands centered at 904–1,103 cm^{-1} are assigned to C–O groups. Moreover, the bands that appeared at 1,025–1,194 cm^{-1} are usually attributed to C–O–C stretching vibrations [31]. Besides, the bands at 1,469; 1,474; 1,594;

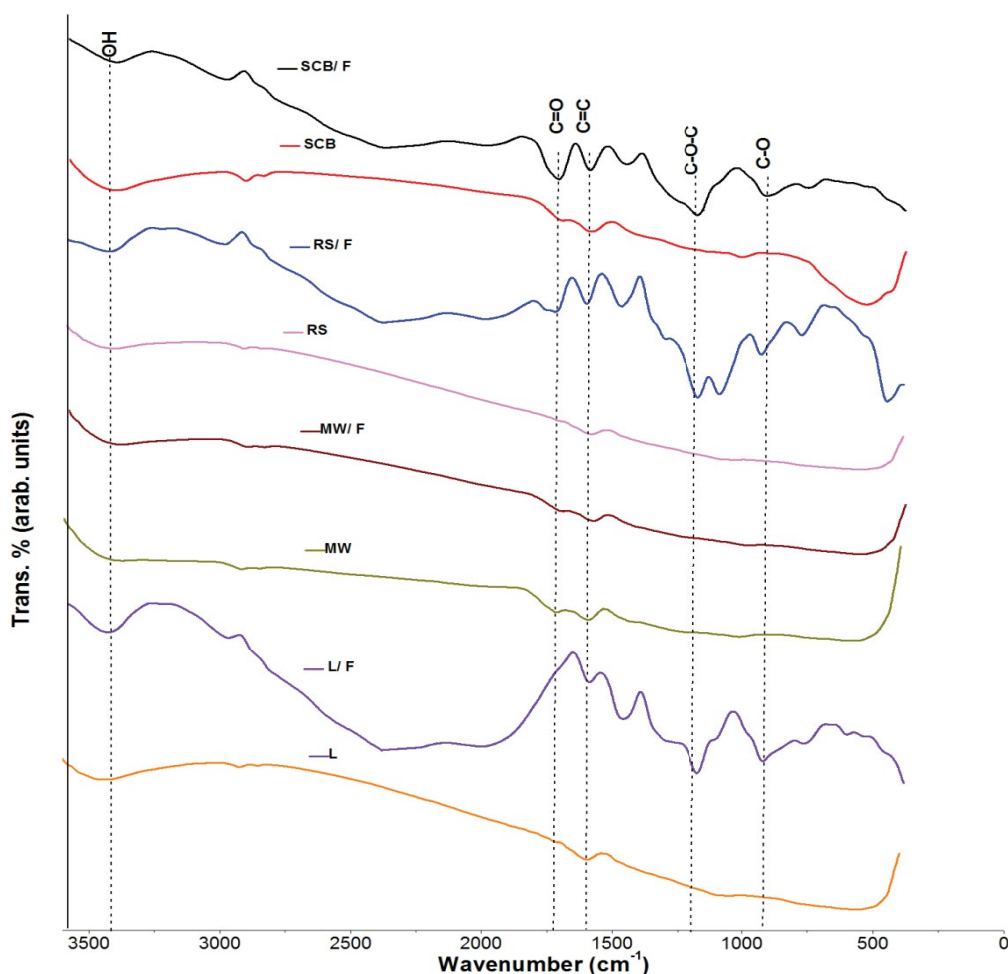


Fig. 3. FT-IR spectra of GOs from SCB/F, SCB, RS/F, RS, MW/F, MW, L/F, and L.

and $1,479\text{ cm}^{-1}$ for SCB/F, L/F, L, and RS/F, respectively are assigned to O=C=O of carboxyl group [17].

The strong peak centered at $3,403\text{--}3,443\text{ cm}^{-1}$ can be attributed to the O–H stretching vibrations of the C–OH groups and water [17,31]. Contrary to the findings of Somanathan et al. [17] we did not find strong and sharp OH peak but it was a broader one.

Finally, it is important to note that the intensity of the wide peak associated to the C–OH stretching vibration (forming hydrogen bonds between GO layers and between GO and water molecules and causing, in turn, the hydrophilic moieties of the sample) is closely related to the oxygen content in the samples [28]. The present findings confirm the oxidation of agro wastes as the ideas of Somanathan et al. [17] which concluded that agro wastes could be oxidized into GO.

The band at $2,991\text{ cm}^{-1}$ can be attributed to C–H stretching. This band was chosen as an internal standard to determine the relative absorbance (RA). The RA of the O–H is 3.20, 1.39, 0.89, 1.0, 0.93, 0.80, 1.09, and 3.46. While the intensity of the C=O is 14.70, 2.80, 0.18, 11.73, 3.58, 1.96, 0.05, and 4.04 for SCB/F, SCB, RS/F, RS, MW/F, MW, L/F, and L respectively. On the other hand, RA of the C–OH is 17.94, 4.74, 1.81, 12.35, and 1.93 for SCB/F, SCB, L/F, L, and RS/F,

respectively. The RA of the C–O–C is 22.08, 4.91, 2.14, 10.38, and 2 for SCB/F, SCB, L/F, L, and RS/F, respectively.

The RA of the O–H, C=O, C–OH, and C–O–C of absorption bands is obviously higher for SCB/F sample. This means that many oxygen groups were found in SCB/F than other GO samples prepared from other different sources. The bands of the C–O and C–O–C stretching vibrations are disappeared in RS, MW, and MW/F which indicates the low level of oxidation of these samples.

RA decreasing of OH, C=O, C–OH, and C–O–C stretching in SCB, L/F, L, RS, and RS/F indicates that C–OH still exist, but in lower proportion than SCB/F. In general, the large numbers of the hydrophilic functional groups on GO surface resulted in higher hydrophilicity and the better water dispersibility of the SCB/F sample [32]. The differences between SCB/F and SCB samples in Raman and IR spectra prove the formation of GO in the case SCB/F, while incomplete oxidation in case of SCB yielded a majority of graphitic carbon.

3.3. SEM and TEM analysis

Fig. 4 depicts the TEM images of the synthesized GOs from the oxidation of different agro wastes. It is clearly seen

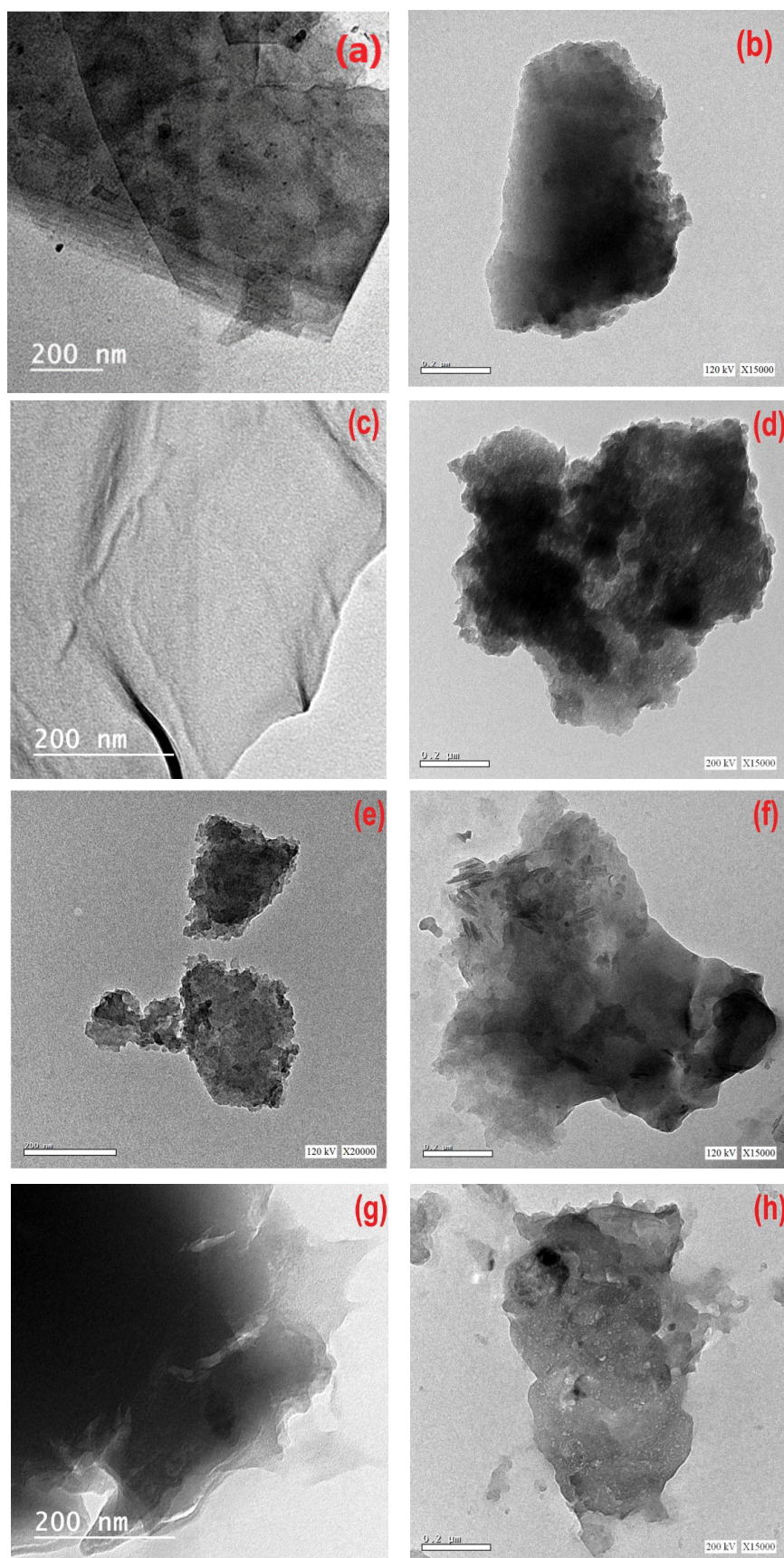


Fig. 4. TEM of GO obtained from (a) SCB/F, (b) SCB, (c) RS/F, (d) RS, (e) MW/F, (f) MW, (g) L/F, and (h) L.

that there are various morphologies of GOs produced. The images reveal that all the as-prepared GOs samples are in sheet-like nature. The color gradient on the edges of the sheets is further proof that GO consists of a few layers of sheets that stack together [33].

Fig. 5 shows SEM images of the prepared GO samples through the oxidation of the raw materials at 300°C for 10 min. The morphology of the synthesized GO samples is sheets randomly aggregated with rounded folds. Additionally, Fig. 5 shows that all samples consist of layers with different transparencies; it may be attributed to the number of layers [34]. The surface of SCB/F, SCB, and L/F was relatively flat compared with other samples. This corrugation of GO sheets is attributed to the disruption of the planar sp² carbon sheets by the introduction of sp³-hybridized carbon upon oxidation. The presence of residual H₂O molecules tightly bound with the carboxyl or hydroxyl group of GO may also lead to this morphology [33]. While the rugged surface of RS and L samples can be due to the distortion of the surface during the drying process. On the other hand, pores size in the synthesized GOs were 250.9, 295.6, 217.9, 39.0, 888.2, and 702.9 nm for SCB/F, SCB, RS/F, MW/F, MW, and L respectively. The pore size of RS and L/F have not appeared in SEM images. This may be due to the dryness of the sample and also it appeared to stick together like tiny pellets that took the shape of the crucible they were dried in.

EDX analysis shows that different elements in weight percentage are found as depicted in Fig. 6. Generally, amounts of C, O, and N elements are higher than other elements (Si, S, Na, Cl, and K) in the prepared GOs. These results reveal that, obtained GOs contain some impurities of amorphous carbon and metals.

3.4. Effect of contact time on Ni(II) adsorption

Different types of GO (SCB/F, SCB, RS/F, RS, MW/F, MW, L/F, and L) were examined for the removal of Ni(II). The effect of contact time on adsorption experiments was studied at different times, namely 15, 30, 45, 60, 75, and 90 min. As shown in Fig. 7 the affinity of GO types towards Ni(II) was different. The removal of Ni(II) by GO adsorbents was found to be fast at initial due to the presence of more active sites [35]. The removal rate became slow and there is no noticeable increase in the adsorption rate observed after 75, 30, 30, 30, 15, 15, 30, and 45 min. (optimum time for adsorption process of Ni(II) on GO at 25°C) for SCB/F, SCB, RS/F, RS, MW/F, MW, L/F, and L, respectively. Although metal-ligand coordinating bonds are formed, the number of ligands per metal is lower than that of stable complexes. As the adsorption proceeds, the metals absorbed rearrange the coordinating environment around the functional groups. The extra Ni(II) are released into the solution as the equilibrium complexes take away their ligands [35].

The adsorption of Ni(II) to SCB/F was found to be much higher than other types of GO ($R\% = 76.05$) and stable until 75 min. This can be attributed to the presence of high oxygen content on the G sheets in the case of SCB/F. Accordingly, the oxygen-containing functional groups on G materials played critical roles in the adsorption of Ni(II) in aqueous solutions [32]. For other samples after a definite

time, the adsorption rate started to decrease due to the leaching process which proving that the samples were not having the same morphology of GO.

3.5. Effect of temperature on Ni(II) adsorption

The effect of temperature on adsorption capacity of Ni(II) on GO surface was performed from 298 to 328 K. All adsorption experiments were performed at fixed contact time (30 min). As shown in Fig. 8, when the temperature increases from 298 to 328 K, the removal of Ni(II) by RS and MW/F surfaces decreases suggesting that the interaction between Ni(II) and RS and MW/F is an exothermic process [36]. This can be explained by the thickness of the boundary layer minimized at high temperature, due to the increased tendency of Ni(II) to escape from the GO surface to the solution phase (weak adsorption interaction between GO surface and Ni(II)), which involves physical adsorption [37].

On the other hand, the removal of Ni(II) by SCB/F, SCB, RS/F, MW, L/F, and L increased with increasing temperature suggesting that adsorption between Ni(II) and SCB/F, SCB, RS/F, MW, L/F, and L is an endothermic process [36]. This can be explained by the nature of the GO molecules. Increasing the temperature will increase the rate of diffusion of Ni(II) across the external boundary layer and in the internal pores of GO particle. The adsorption of Ni(II) by GO may involve physical and chemical adsorption due to higher temperature, thus an increase in active sites occurs due to bond rupture [38]. In another words, the endothermic reaction is due to enlargement of pore size and activation of GO surface [39]. The difference in adsorption attitude of Ni by the prepared samples as shown in Fig. 8, proving that the samples were not having the same morphology of GO.

3.6. Effect of initial concentration on Ni(II) adsorption

The effect of the initial concentration of Ni(II) in solution was considered (Fig. 9). The removal experiments were performed using various initial concentrations from 15, 20, 25, and 30 mg/L at a steady contact time of 30 min. It is evident from Fig. 9 that the percentage of Ni(II) removal decreased with increasing the initial concentration of Ni(II). The number of exchangeable sites in GO structure and the ratio of Ni(II) to GO are reasons for the decrease in the percentage of Ni(II) removal with increasing initial concentration of Ni(II). As the ratio of Ni(II) to GO increases, the exchangeable sites in GO are saturated, resulting in decreasing of removal percentage. While the percentage Ni(II) removal for SCB/F, SCB, RS/F, RS, L/F, L, MW/F, and MW, respectively was found to be 72.38%, 72.63%, 68.88%, 72.67%, 67.89%, 63.75%, 69.09%, and 70.01% at 15 mg/L of initial concentration, this value was 34.67%, 39.22%, 25.50%, 51.16%, 58.47%, 42.67%, 37.13%, and 45.21% for that of 30 mg/L. This may be attributed to the lack of sufficient surface area to accommodate excess Ni(II) available in the solution and the saturation of adsorption sites at high concentrations (20, 25, and 30 mg/L) [40].

3.7. Kinetic modeling

In order to achieve the controlling rate mechanism of the adsorption processes such as mass transfer and chemical

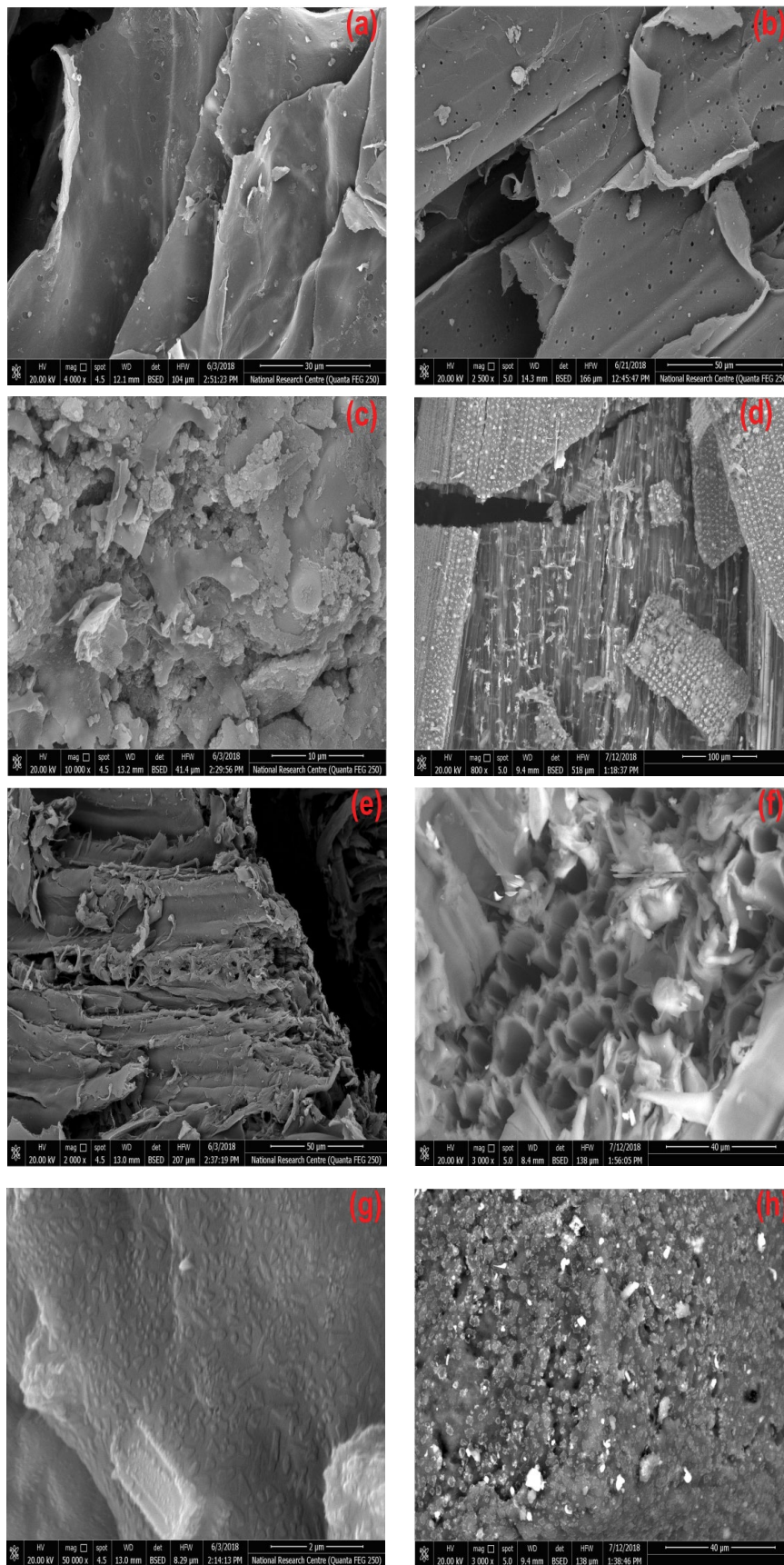


Fig. 5. SEM of GO obtained from (a) SCB/F, (b) SCB, (c) RS/F, (d) RS, (e) MW/F, (f) MW, (g) L/F, and (h) L.

reaction, the pseudo-first-order and pseudo-second-order equations are utilized to model the kinetics data of Ni(II) adsorption onto GO surface [39]. The first and second order equations were applied to the data derived from the effect of time on adsorption.

Pseudo-first-order is based on the hypothesis that physisorption is the rate determining step and it is given in Eq. (2).

$$\ln[q_e - q_t] = \ln q_e - K_1 t \tag{2}$$

where q_e and q_t are the amounts of Ni(II) adsorbed (mg/g) at equilibrium and time t , respectively, K_1 (min^{-1}) is the pseudo-first-order rate constant of adsorption. The previous variables and the regression coefficient (R^2) obtained is given in Table 2 [39].

Pseudo-second-order is based on the hypothesis that chemisorption is the rate determining step and it is given in Eq. (3).

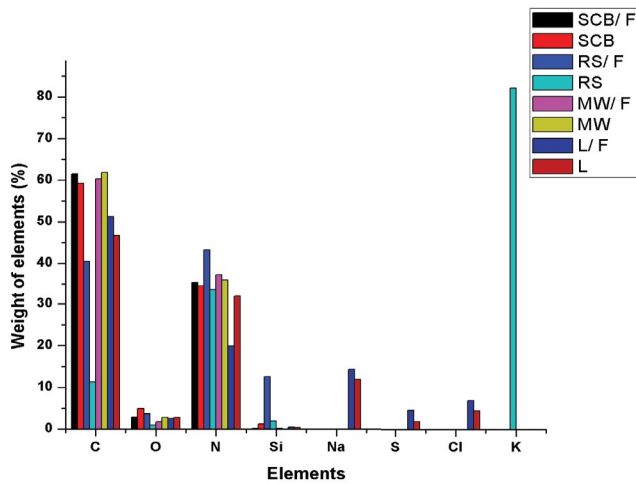


Fig. 6. EDX histogram of the elements present in the prepared GOs.

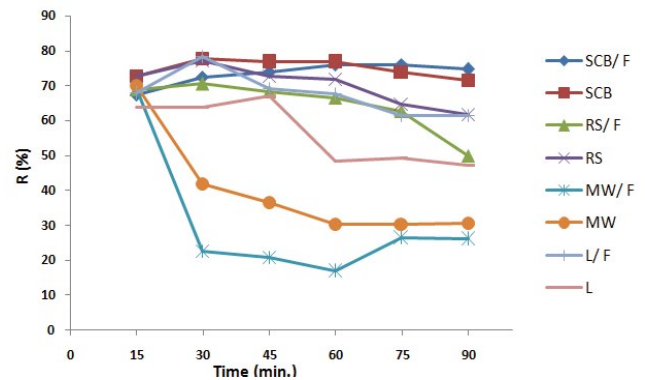


Fig. 7. Effect of contact time on the removal of the Ni²⁺ by different GOs.

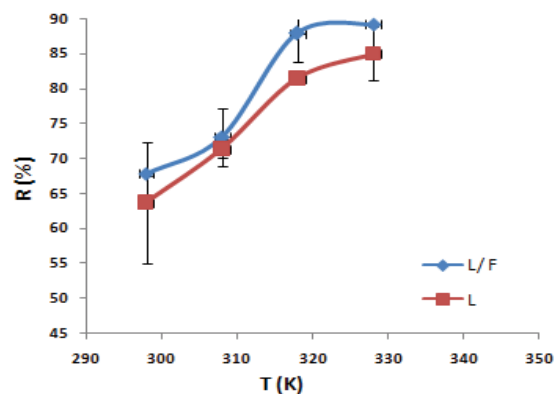
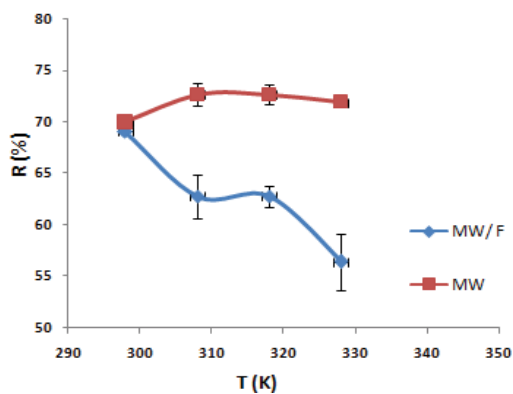
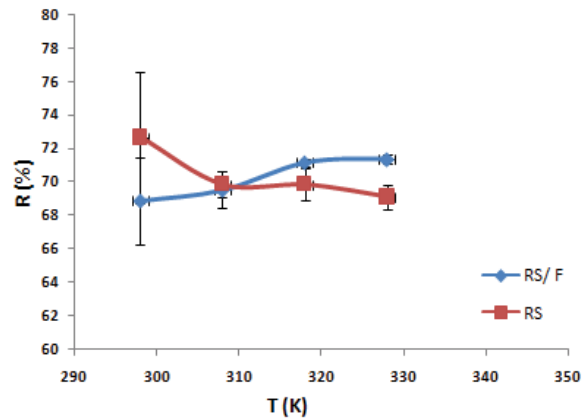
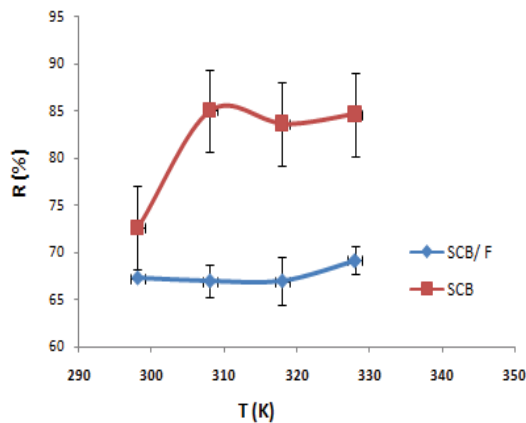


Fig. 8. Effect of temperature on the removal of the Ni²⁺ by different GOs.

Table 2

Comparison between the estimated adsorption rate constants, rate constants and correlation coefficients associated with the pseudo-first-order and the pseudo-second-order rate

Kinetic model	Parameter	Adsorbent							
		SCB/F	SCB	RS/F	RS	MW/F	MW	L/F	L
Pseudo-first-order	q_{exp}	13.468	13.702	12.437	13.59	12.179	12.34	13.805	11.806
	q_{calc}	12.056	13.500	13.775	14.095	8.051	11.397	13.471	12.776
	K_1	0.37	0.0004	0.0038	0.0025	0.0096	0.0101	0.0024	0.0049
	R^2	0.647	0.128	0.688	0.749	0.312	0.754	0.551	0.725
Pseudo-second-order	q_{calc}	4.084	50.061	5.864	5.0099	16.637	9.549	5.586	9.013
	K_2	0.7083	0.141	0.805	3.442	0.057	0.3212	0.4698	0.0989
	R^2	0.981	0.946	0.960	0.986	0.909	0.944	0.937	0.965

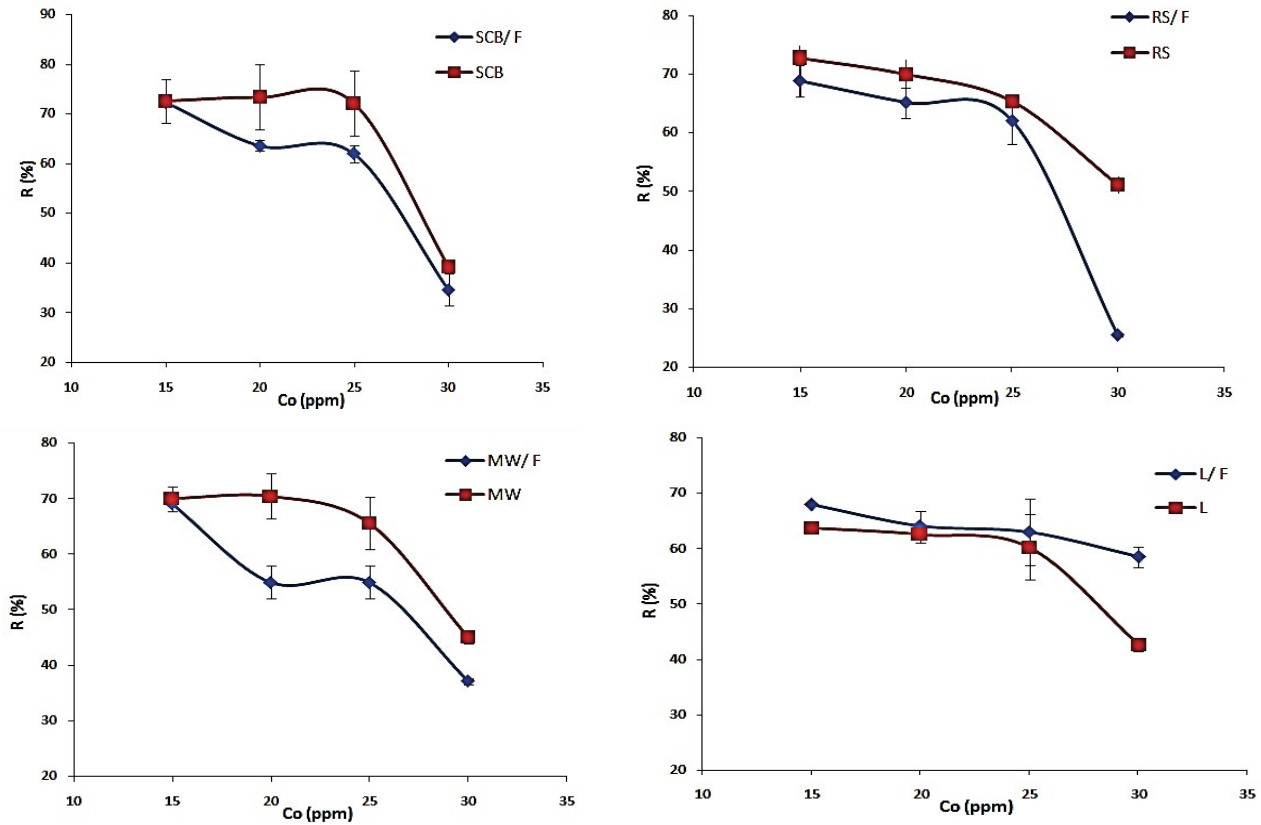


Fig. 9. Effect of initial Ni²⁺ ion concentration on the adsorption process by GO surface.

$$\frac{t}{q_t} = \frac{1}{K_2 q_e^2} + \frac{t}{q_e} \quad (3)$$

where K_2 (g/mg/min) is the rate constant of pseudo-second-order adsorption. Values of q_e^2 and K_2 were calculated from the slope and intercept of the plot of t/q_t against t and are shown in Fig. 10b. In chemisorptions (i.e., chemical adsorption), the Ni(II) stick to the GO surface by chemical bond (usually covalent) and prefer to find sites that maximize their coordination number with the surface [41].

With respect to the values of R^2 presented in Table 2, it is seen that the pseudo-second-order model gave a better fit to the adsorption data than the first-order one. This elucidates that surface processes involving chemisorptions adsorption of Ni(II) by GO [39].

3.8. Adsorption isotherm

The adsorption isotherm provides information on how the adsorbed molecules distribute between the liquid phase and the solid phase when the adsorption process reaches an equilibrium state (i.e., the adsorption mechanisms, the

surface properties, and affinities of the adsorbent) [36,39]. R^2 is used to determine the best-fitting isotherm. In the current study, the adsorption equilibrium data were fitted to Langmuir and Freundlich isotherm models.

3.8.1. Langmuir isotherm model

It is the simplest type, based on the vision that every adsorption site is equivalent and independent; the ability of a molecule to bind is independent of neighboring sites that are occupied or not [42]. The Langmuir model is given by Eq. (4).

$$\frac{C_e}{q_e} = \frac{1}{Kq_m} + \frac{C_e}{q_m} \tag{4}$$

where q_m (mg/g) is the maximum removal capacity [39].

3.8.2. Freundlich model

It describes the non-ideal and reversible adsorption (i.e., an infinite supply of unreacted GO sites) and prefers to represent heterogeneous materials better than other models. The Freundlich model is given by Eq. (5).

$$\log q_e = \log K_f + \frac{1}{n} \log C_e \tag{5}$$

where K_f is adsorption capacity [38]. Langmuir isotherm restricted to the formation of the monolayer in contrast to Freundlich isotherm which can be applied to multilayer adsorption, with non-uniform distribution of adsorption heat and affinities over the heterogeneous surface.

The higher K_f indicates that the adsorbent being more reactive [42]. All GO isotherms fit well with the Langmuir model, since R^2 was high (Fig. 11 and Table 3).

Langmuir parameters of GO indicated a q_m of 10.99, 7.75, 8.01, 6.34, 7.07, and 9.60 mg/g for SCB/F, SCB, RS/F, RS, MW/F, MW, and L, respectively. So, it can be derived that SCB/F, RS/F, RS, MW/F, MW, L/F, and L surface is homogeneous; and surface adsorption is often done in the form of a monolayer.

4. Conclusions

The optimized values of contact time of Ni(II) were found to be 75, 30, 30, 30, 15, 15, 30, and 45 min for SCB/F, SCB, RS/F, RS, MW/F, MW, L/F, and L, respectively with and 15 mg/L as initial concentration. Ongoing through the

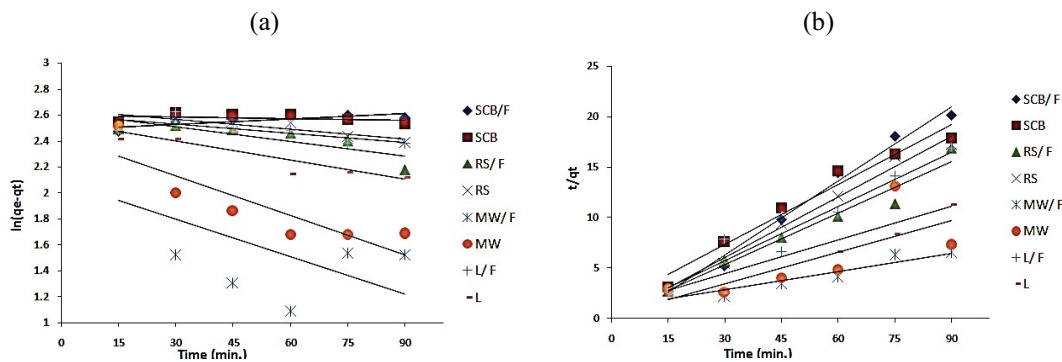


Fig. 10. Kinetic parameters of (a) pseudo-first-order and (b) pseudo-second-order reaction for Ni²⁺ adsorbed onto GO at different time intervals.

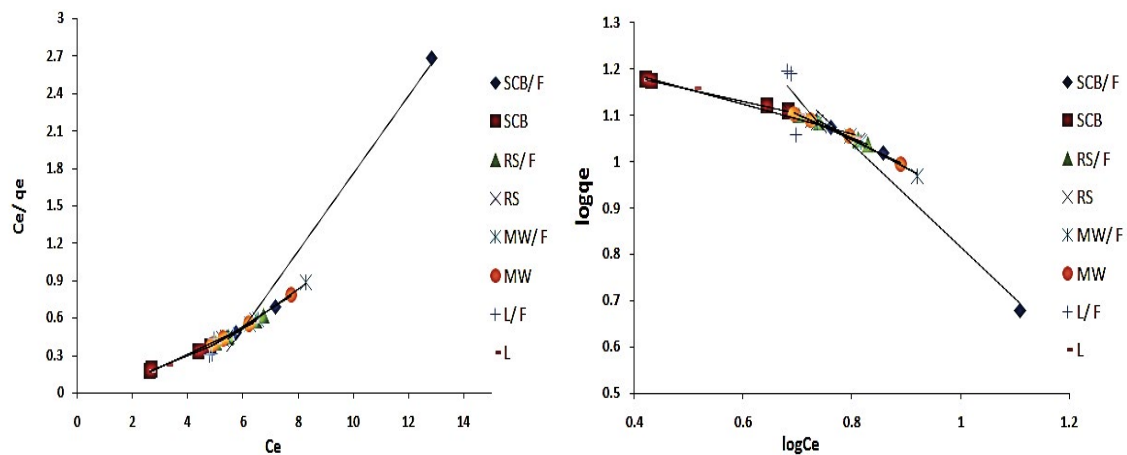


Fig. 11. Langmuir isotherm (left) and Freundlich isotherm (right) of Ni²⁺ ions on GO surfaces. Initial concentration 15 mg/L; adsorbent dosage: 20 mg; time: 30 min.

Table 3

Langmuir and Freundlich models parameters for adsorption of Ni(II) on GO surfaces. Initial concentration 15 mg/L; adsorbents dosage 20 mg; time 30 min

Kinetic model	Parameter	Adsorbent							
		SCB/F	SCB	RS/F	RS	MW/F	MW	L/F	L
Langmuir	q_m (mg/g)	3.22	10.99	7.75	8.01	6.34	7.07	5.66	9.60
	R^2	0.984	0.963	0.999	0.998	0.994	0.995	0.679	0.994
Freundlich	K_f (mg ^(1-1/n) g ⁻¹ L ^{1/n})	6.87	3.61	4.28	4.20	4.78	4.46	8.36	3.73
	R^2	0.974	0.997	0.998	0.995	0.989	0.991	0.400	0.98

impact of temperature it was showed that, when the temperature was increased from 298 to 328 K, the removal of Ni(II) by RS and MW/F surfaces decreased. While the removal of Ni(II) by SCB/F, SCB, RS/F, MW, L/F, and L increased with increasing temperature suggesting that this adsorption is an endothermic process. With respect to the values of R^2 , the pseudo-second-order model gave a better fit to the adsorption than the first-order one. But the q_m values obtained in the pseudo-first-order are still suitable for describing the kinetics of Ni(II) sorption. Langmuir and Freundlich isotherm models were used and the results clearly reveal that the adsorption of Ni(II) on GO surfaces was well fitted and found to be in good agreement with Langmuir isotherm model.

Acknowledgment

The authors acknowledge the Academy of Scientific Research and Technology (ASRT), Egypt and Czech Academy of Sciences, for financial support of the bilateral research activities.

References

- [1] A. Whelan, N.B. McGuinness, M. Garvey, H. John, C. Zao, G. Zhang, D.D. Dionysiou, J.A. Byrne, S.C. Pillai, Nanotechnology Solutions for Global Water Challenges, S. Ahuja, K. Hristovski, J. de Andrade, B. Loganathan, D. Dionysiou, Eds., Water Challenges and Solutions on a Global Scale, ACS Symposium Series, American Chemical Society, Washington, DC, 2015.
- [2] S. Raghav, R. Painuli, D. Kumar, Threats to Water: Issues and Challenges Related to Ground Water and Drinking Water, M. Naushad, Ed., A New Generation Material Graphene: Applications in Water Technology, Springer, 2019, pp. 1–19.
- [3] T. Tatarchuk, M. Bououdina, B. Al-Najar, R.B. Bitra, Green and Ecofriendly Materials for the Remediation of Inorganic and Organic Pollutants in Water, M. Naushad, Ed., A New Generation Material Graphene: Applications in Water Technology, Springer, Cham, 2019, pp. 69–110.
- [4] K. Padmaja, J. Cherukuri, M. Anji Reddy, Conventional to cutting edge technologies in drinking water purification—a review, Int. J. Innovative Res. Sci. Eng. Technol., 3 (2014) 9375–9385.
- [5] R. Baby Shaikh, B. Saifullah, F. Rehman, Greener method for the removal of toxic metal ions from the wastewater by application of agricultural waste as an adsorbent, Water, 10 (2018) 1316.
- [6] A. Aghigh, V. Alizadeh, H.Y. Wong, M.S. Islam, N. Amin, M. Zaman, Recent advances in utilization of graphene for filtration and desalination of water: a review, Desalination, 365 (2015) 389–397.
- [7] S. Bolisetty, M. Peydayesh, R. Mezzenga, Sustainable technologies for water purification from heavy metals: review and analysis, Chem. Soc. Rev., 48 (2019) 463–487.
- [8] H. Ren, D.D. Kulkarni, R. Kodiyath, W. Xu, I. Choi, V.V. Tsukruk, Competitive adsorption of dopamine and rhodamine 6G on the surface of graphene oxide, ACS Appl. Mater. Interfaces, 6 (2014) 2459–2470.
- [9] E. Chigo-Anota, M. Salazar-Villanueva, H. Hernández-Cocolezzi, Electronic properties of boron nitride oxide nanoclusters, J. Nanosci. Nanotechnol., 11 (2011) 5515–5518.
- [10] G. Gollavelli, C.-C. Chang, Y.-C. Ling, Facile synthesis of smart magnetic graphene for safe drinking water: heavy metal removal and disinfection control, ACS Sustainable Chem. Eng., 1 (2013) 462–472.
- [11] P.T.L. Huong, N. Tu, H. Lan, L.H. Thang, N.V. Quy, P.A. Tuan, N.X. Dinh, V.N. Phan, A.-T. Le, Functional manganese ferrite/graphene oxide nanocomposites: effects of graphene oxide on the adsorption mechanisms of organic MB dye and inorganic As(V) ions from aqueous solution, RSC Adv., 8 (2018) 12376–12389.
- [12] L. Bautista-Patacsil, J. Lazarte, R. Dipasupil, G. Pasco, R. Eusebio, A. Orbecido, R. Doong, Deionization utilizing reduced graphene oxide-titanium dioxide nanotubes composite for the removal of Pb²⁺ and Cu²⁺, J. Environ. Chem. Eng., (in Press), <https://doi.org/10.1016/j.jece.2019.103063>.
- [13] M.Y. Akram, S. Ahmed, L. Li, N. Akhtar, S. Ali, G. Muhyodin, X.-Q. Zhu, J. Nie, N-doped reduced graphene oxide decorated with Fe₃O₄ composite: stable and magnetically separable adsorbent solution for high performance phosphate removal, J. Environ. Chem. Eng., 7 (2019) 103137.
- [14] T. Cheminski, T.F. Neves, P.M. Silva, C.H. Guimarães, P. Preddiger, Insertion of phenyl ethyleneglycol units on graphene oxide as stabilizers and its application for surfactant removal, J. Environ. Chem. Eng., 7 (2019) 102976.
- [15] S. Saha, M. Venkatesh, H. Basu, M.V. Pimple, R.K. Singhal, Recovery of gold using graphene oxide/calcium alginate hydrogel beads from a scrap solid state detector, J. Environ. Chem. Eng., 7 (2019) 103134.
- [16] G. Zhou, C. Liu, Y. Tang, S. Luo, Z. Zeng, Y. Liu, R. Xu, L. Chu, Sponge-like polysiloxane-graphene oxide gel as a highly efficient and renewable adsorbent for lead and cadmium metals removal from wastewater, Chem. Eng. J., 280 (2015) 275–282.
- [17] T. Somanathan, K. Prasad, K. Ostrikov, A. Saravanan, V.M. Krishna, Graphene oxide synthesis from agro waste, Nanomaterials, 5 (2015) 826–834.
- [18] H.B.A. Hassan, M.R. El Gebaly, S.S. Abdul Ghani, Y.M.M. Hussein, An economic study of recycling agricultural wastes in Egypt, Middle East J. Agric. Res., 3 (2014) 592–608.
- [19] C. Zhuo, J.O. Alves, J.A.S. Tenorio, Y.A. Levendis, Synthesis of carbon nanomaterials through up-cycling agricultural and municipal solid wastes, Ind. Eng. Chem. Res., 51 (2012) 2922–2930.
- [20] Z. Wang, H. Ogata, S. Morimoto, J. Ortiz-Medina, M. Fujishige, K. Takeuchi, H. Muramatsu, T. Hayashi, M. Terrones, Y. Hashimoto, M. Endo, Nanocarbons from rice husk by microwave plasma irradiation: from graphene and carbon nanotubes to graphenated carbon nanotube hybrids, Carbon, 94 (2015) 479–484.
- [21] L. Sun, C. Tian, M. Li, X. Meng, L. Wang, R. Wang, J. Yin, H. Fu, From coconut shell to porous graphene-like nanosheets

- for high-power supercapacitors, *J. Mater. Chem. A*, 1 (2013) 6462–6470.
- [22] V.F. Lofly, N.A. Fathy, A.H. Basta, Novel approach for synthesizing different shapes of carbon nanotubes from rice straw residue, *J. Environ. Chem. Eng.*, 6 (2018) 6263–6274.
- [23] A.M.P. Arnau, H.G. Gómez, E.S. Cortezón, J.M.D. Sánchez, Method for Obtaining Solid Graphene Samples or Suspensions, European Patent Application EP2924005A1, 2015.
- [24] B. Goodell, X. Xie, Y. Qian, G. Daniel, M. Peterson, J. Jellison, Carbon nanotubes (CNTs) produced from natural cellulosic materials, *J. Nanosci. Nanotechnol.*, 8 (2008) 2472–2474.
- [25] A.K. Mishra, S. Ramaprabhu, Functionalized graphene sheets for arsenic removal and desalination of sea water, *Desalination*, 282 (2011) 39–45.
- [26] S. Kellici, J. Acord, J. Ball, H.S. Reehal, D. Morgan, B. Saha, A single rapid route for the synthesis of reduced graphene oxide with antibacterial activities, *RSC Adv.*, 4 (2014) 14858–14861.
- [27] S.R.A. Alazmi, S.P. Patole, P.M. Costa, Comparative study of synthesis and reduction methods for graphene oxide, *Polyhedron*, 116 (2016) 153–161.
- [28] A. Romero, M. Lavin-Lopez, L. Sanchez-Silva, J. Valverde, A. Paton-Carrero, Comparative study of different scalable routes to synthesize graphene oxide and reduced graphene oxide, *Mater. Chem. Phys.*, 203 (2018) 284–292.
- [29] O. Akhavan, K. Bijanzad, A. Mirsepah, Synthesis of graphene from natural and industrial carbonaceous wastes, *RSC Adv.*, 4 (2014) 20441–20448.
- [30] D. Chen, H. Feng, J. Li, Graphene oxide: preparation, functionalization, and electrochemical applications, *Chem. Rev.*, 112 (2012) 6027–6053.
- [31] H. Nassef, M. Hagar, Z. Malek, A. Othman, Uptake of tyrosine amino acid on nano-graphene oxide, *Materials*, 11 (2018) 68.
- [32] J. Wang, B. Chen, Adsorption and coadsorption of organic pollutants and a heavy metal by graphene oxide and reduced graphene materials, *Chem. Eng. J.*, 281 (2015) 379–388.
- [33] A.T. Smith, A.M. LaChance, S. Zeng, B. Lium, L. Sun, Synthesis, properties, and applications of graphene oxide/reduced graphene oxide and their nanocomposites, *Nano Mater. Sci.*, 1 (2019) 31–47.
- [34] A. Shalaby, D. Nihtianova, P. Markov, A.D. Staneva, R.S. Iordanova, Y.B. Dimitrie, Structural analysis of reduced graphene oxide by transmission electron microscopy, *Bulg. Chem. Commun.*, 1 (2015) 291–295.
- [35] J.-Y. Lee, C.-H. Chen, S. Cheng, H.-Y. Li, Adsorption of Pb(II) and Cu(II) metal ions on functionalized large-pore mesoporous silica, *Int. J. Environ. Sci. Technol.*, 13 (2016) 65–76.
- [36] P.S. Kumar, K. Ramakrishnan, S.D. Kirupha, S. Sivanesan, Thermodynamic and kinetic studies of cadmium adsorption from aqueous solution onto rice husk, *Braz. J. Chem. Eng.*, 27 (2010) 347–355.
- [37] M.H. Jnr, A.I. Spiff, Effects of temperature on the sorption of Pb²⁺ and Cd²⁺ from aqueous solution by *Caladium bicolor* (Wild Cocoyam) biomass, *Electron. J. Biotechnol.*, 8 (2005) 43–50.
- [38] G.M. Al-Senani, F.F. Al-Fawzan, Adsorption study of heavy metal ions from aqueous solution by nanoparticle of wild herbs, *Egypt. J. Aquat. Res.*, 44 (2018) 187–194.
- [39] F.A. Dawodu, K. Akpomie, P.C.N. Ejikeme, Equilibrium, thermodynamic and kinetic studies on the adsorption of lead(II) from solution by “Agbani clay”, *Res. J. Eng. Sci.*, 1 (2012) 9–17.
- [40] M. Shafiq, A. Alazba, M. Amin, Removal of heavy metals from wastewater using date palm as a biosorbent: a comparative review, *Sains Malaysiana*, 47 (2018) 35–49.
- [41] P.S. Kumar, K. Kirthika, Equilibrium and kinetic study of adsorption of nickel from aqueous solution onto bael tree leaf powder, *J. Eng. Sci. Technol.*, 4 (2009) 351–363.
- [42] K.B. Payne, T.M. Abdel-Fattah, Adsorption of divalent lead ions by zeolites and activated carbon: effects of pH, temperature, and ionic strength, *J. Environ. Sci. Health., Part A*, 39 (2004) 2275–2291.